Strain Rate Effects on Fracture Behavior of Austempered Ductile Irons

N.B. When citing this work, cite the original published paper.

(article starts on next page)

Strain rate effects on fracture behavior of austempered ductile irons

A. Ruggiero, N. Bonora, D. Gentile, G. Iannitti, G. Testa, M. Hörnqvist Colliander, S. Masaggia, and F. Vettore

Articles you may be interested in

Numerical simulation and validation of damage in AA1100 aluminum symmetric Taylor impact (ROR)
AIP Conference Proceedings **1979**, 070006 (2018); 10.1063/1.5044815

The dynamic ductile fracture of high purity copper
AIP Conference Proceedings **1979**, 070032 (2018); 10.1063/1.5044841

Strain Rate Effects on Fracture Behavior of Austempered Ductile Irons

A. Ruggiero[1,a)], N. Bonora[1], D. Gentile[1], G. Iannitti[1], G. Testa[1], M. Hörnqvist Colliander[2], S. Masaggia[3] and F. Vettore[3]

[1]*Department of Civil and Mechanical Engineering, University of Cassino and Southern Lazio, Italy.*
[2]*Applied Physics, Chalmers University of Technology, Gothenburg, Sweden.*
[3]*Zanardi Fonderie SpA, Minerbe, Italy.*

a)Corresponding author: a.ruggiero@unicas.it

Abstract. In this work, the mechanical behavior of the austempered ductile iron (ADI) JS/1050-6 was investigated, with particular attention to the strain rate effects on the material ductility. Tensile tests at different strain rates (up to 10^3 s^{-1}) and temperatures (ranging from 213 to 343 K) were performed. Samples with different geometries, smooth and round notched bars, were used to evaluate the effect of the stress triaxiality level on the strain at fracture. For each configuration, the evolution paths of stress and strain were extracted in the point where failure is expected performing numerical analyses at the continuum scale.

Stress histories were used as input in a micromechanics analysis aimed to analyze the heterogeneous state of stress, determined by the presence of the graphite nuclei, under the different loading conditions obtained in the experiments. The main result is that, under dynamic conditions, the stress field redistribution, due to the adiabatic condition, postpones the failure occurrence, regardless temperature and strain rate effects on the matrix ductility.

INTRODUCTION

Ductile cast irons (DCIs) are widely used in several applications in virtue of their properties of castability, cast dimension stability, and high ductility [1]. For ferritic grades, ductility up to 25% can be reached mainly thanks to the spheroidal shape of the graphite nuclei [2].

Among these, a relative new class is represented by austempered ductile iron (ADIs). Here, the austempering process yields to a very high-strength matrix, consisting of acicular ferrite in carbon-enriched austenite [3, 4, 5]. The excellent properties combination of strength, ductility, toughness and low density puts the ADIs to be a suitable alternative to high-strength steels [6, 7]. Nevertheless, designers show lack of confidence in using ADIs in structural applications, mainly because of the general perception and concern about their intrinsic brittleness that could be promoted by dynamic loading.

Although the mechanical response of these materials has been investigated extensively, as today, information about the strain rate effect on the constitutive behavior is still very limited. Böhme and Reissig [8] performed quasi-static and dynamic tensile tests, up to strain rate of 100 s^{-1}, on ADI 1000 and ADI 1200. They observed an increase in both strength and elongation at fracture with increasing strain rate. Yamamoto et al. [9] investigated the strain rate effects at different temperatures of as-cast and ferritic annealed DCI using Charpy impact test. Myszka et al. [10] analyzed several grades of ADI, austempered at different temperatures, using Taylor's cylinder impact test, with the attempt to determine the effect of dynamic load on the strain driven transformation of matrix phases. No information is available, to the best authors' knowledge, about the mechanism by which the strain rate affects the ADIs ductility.

The aim of this work is to investigate ductile failure mechanisms in the ADI JS/1050-6 under different loading conditions, with particular attention to the strain rate effect, evaluating how the heterogeneous state of stress into the matrix affects the failure process.

To this purpose, the following approach was used. First, tensile tests at different strain rates, temperatures, and stress triaxiality levels were performed. The phenomenological, macroscopic response, in terms of stress-strain curve

and elongation at fracture, was analyzed. For each test, at the point where failure is expected, the evolution paths of stress and strain, at the continuum scale, were determined by means of finite element (FE) simulations.

Then, a FE micromechanics analysis was performed by developing an unit cell model (UCM) that reproduces the periodic microstructure of the ADI. As a matter of fact, the presence of two distinct phases, *i.e.* particles embedded into a matrix, makes this material conceptually a "natural" composite [11] whose resulting properties at the macroscale can be determined from characteristics of the constituents and microstructure topology of the material [12, 13]. Further, if damage mechanisms are accounted for, UCM can predict the occurrence of failure under different loading conditions and stress triaxiality factors [14]. For each test, the stress triaxiality histories, determined at the macroscale, were used as input of the UCM analyses whose performances were verified by comparison with the experiments. Finally, the UCM was used to investigate the stress distribution into the matrix under different loading conditions and its effect on the failure. The main result of the work is the explanation of the mechanism for which, due to a stress redistribution into the matrix, contrary to what is commonly perceived, the ductility of ADIs, and DCIs in general, increases with increasing strain rate.

The main result of this work was to come up with an explanation of the mechanism for which, on contrary to what is commonly perceived, the ductility of the ADIs increases with increasing strain rate.

MATERIAL AND EXPERIMENTS

The material investigated in this work is the ADI JS/1050-6, supplied by Zanardi Fonderie SpA. The material was cast in cylinders of 25 mm diameter and 200 mm long. The material microstructure showed a good nodularity and equally spaced spheroids with an average spheroid diameter of 40 μm, more details can be found in [15]. The austempering heat treatment produces a matrix microstructure consisting of acicular ferrite, which has a body-centered cubic (BCC) crystal structure, in carbon-enriched austenite, with a cace-centered cubic (FCC) structure.

Tensile tests were performed at the temperature of 213, 298, and 343 K at the nominal strain rates of 0.001, 740, and 1200 s^{-1}. Quasi-static tests were performed with an Instron 5586 electromechanical testing machine and the load vs stroke displacement was recorded. At room temperature, strain was measured also using an extensometer with a reference length of 12.5 mm and with digital image correlation (DIC) technique. Dynamic tests were performed with a direct tension split Hopkinson pressure bar (DT-SHPB). At room temperature, in addition to the data obtained from the bars signals, the strain in the sample was measured using in situ DIC by means of high speed camera v7.3 Phantom. More details on experimental setup can be found in [15].

Different geometries of the samples were adopted to vary the stress triaxiality and to investigate its effect on the material ductility. The same minimum section, with a diameter of 3.5 mm, was used for all the specimens in order to avoid any possible scale effect. Uniaxial tensile tests were performed using smooth bars with a length of reduced section of 14 and 6 mm for quasistatic and dynamic tests respectively. Higher stress triaxiality were obtained using round notched bars with notch radii of 1.5, 3.0, and 6.0 mm, labeled as RndA, RndB, and RndC respectively.

Tensile tests on smooth bars show that, for all the investigated strain rates, decreasing the temperature, the work
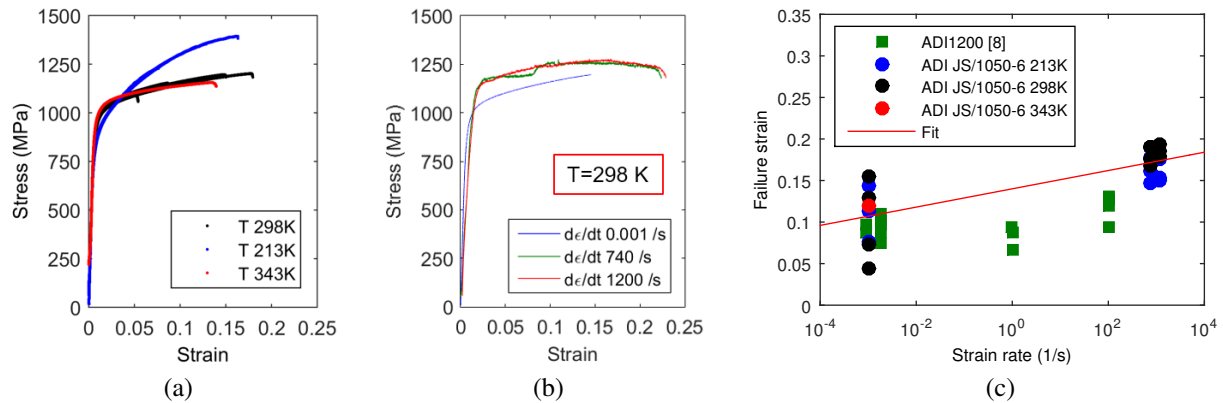

FIGURE 1. (a) Quasi-static stress-strain curves; (b) stress-strain curves at 298 K; (c) failure strain variation with strain rate.

hardening rate increases, whereas the apparent yield strength seems to decrease slightly, Figure 1(a). An increase of the strain rate entails an increase of the yield stress, but it does not affect the hardening rate, Figure 1(b). It is worth noting that, for the higher strain rates, the combination of a higher strength curve, at same slope, and a higher failure strain makes possible to overcome the Considéré's condition and to develop necking, that has no means to occur under quasistatic conditions. Failure strain increases with both temperature and strain rate. Similar results are reported by Böhme and Reissing [8] for the ADI 1200, Figure 1(c).

MICROMECHANICAL MODEL

For the micromechanical analysis, an UCM reproducing the periodic microstructure of the ADI was developed with the FE commercial code MSC Marc 2016.0.0, assuming an axisymmetric configuration. The spheroid and the matrix were simulated as separated deformable bodies. The plane-remain-plane conditions were applied to the top and right side of the cell. Friction in the contact between the matrix and the spheroid interface was considered negligible.

From the constitutive point of view, the graphite nodule was modeled as elastic body. The strength of the ausferrite matrix was described with the model proposed by Iannitti *et al.* [15] that is able to describe the overall mechanical behavior that comes from a mixed FCC and BCC microstructure:

$$\sigma_y = \left(\sigma_{y_0} + A_2 \varepsilon_p^{b_2} + A_1(T)\varepsilon_p^{b_1(T)}\right)\left(1 + C \ln \frac{\dot{\varepsilon}}{\dot{\varepsilon}_0}\right), \tag{1}$$

where $\dot{\varepsilon}_0$ is the reference strain rate and the coefficients A_1 and b_1 are function of temperature according to the following laws:

$$A_1(T) = D + E \exp\left(-\frac{T}{T_1}\right), \tag{2}$$

$$b_1(T) = G + H \exp\left(-\frac{T}{T_2}\right). \tag{3}$$

The coefficients for the ausferrite matrix of ADI 1050 are given in Table 1.

TABLE 1. Strength model coefficients for the ausferrite matrix [15].

σ_{y_0} (MPa)	A_2 (MPa)	b_2	C	D (MPa)	E (MPa)	T_1 (K)	G (MPa)	H (MPa)	T_2 (K)	$\dot{\varepsilon}_0$ (s^{-1})
820	1400	1	0.007	569.1	7.74E4	53.37	3.6E-2	5.38	79.13	1E-3

For DCIs, damage consists of two main mechanisms [2]: debonding of the matrix from the spheroids; nucleation and growth of micro-pores within the matrix. Debonding occurs when the applied stress overcomes the residual stress at the interface resulting from the cooling process. To account for this mechanism, in the simulations, the cooling phase was modeled in order to calculate the proper residual stress field.

Damage into the ductile matrix was described with the Bonora's damage model [16], developed in the framework of the continuum damage mechanics [17]. According to the model formulation, damage develops as a function of the total accumulated active plastic strain, *i.e.* the plastic strain accumulated under a positive (tensile) state of stress [18], and degrades the material properties in terms of stiffness modulus [19]. The damage evolution law,

$$\dot{D} = \alpha \left(\frac{D_{cr}^{1/\alpha}}{\ln(\varepsilon_f/\varepsilon_{th})}\right) R_v \left(D_{cr} - D\right)^{\frac{\alpha-1}{\alpha}}, \tag{4}$$

requires the determination of four coefficients, all with a specific physical meaning: the threshold strain, ε_{th}, at which damage processes are activated; the theoretical failure strain under uniaxial stress, ε_f, at which ductile failure would occur; the critical damage, D_{cr}, at which failure occurs; the damage exponent, α, that controls the shape of damage evolution with plastic strain. The evolution law accounts for stress triaxiality according with:

$$R_v = \frac{2}{3}(1 + \nu) + 3(1 - 2\nu)\left(\frac{\sigma_m}{\sigma_{eq}}\right)^2. \tag{5}$$
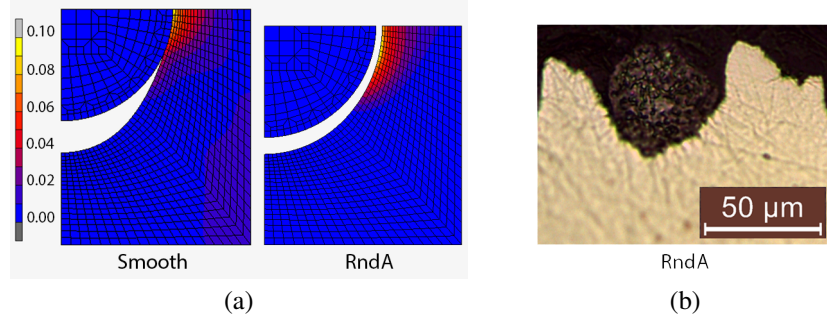
FIGURE 2. (a) Damage contours and deformation of the unit cell at fracture initiation (vertical applied load); (b) debonding morphology on the fracture surface.
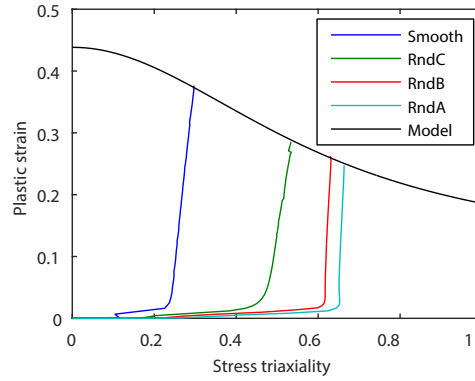

FIGURE 3. Strain vs stress triaxiality paths and matrix failure locus for different specimen geometries.

ANALYSES

First, the UCM was tested under the different states of stress obtained with the quasistatic tensile tests on smooth and round notched geometries. The simulations of these tests show that the morphology of the matrix debonding from the spheroids depends on the stress triaxiality level, Figure 2(a). For the uniaxial stress condition, the debonding is strongly oriented in the load direction, with the matrix squeezed against the spheroid in the orthogonal direction. Increasing the stress hydrostatic component (*e.g.* using RndA specimen geometry) entails a more spherical debonding. The micrography in Figure 2(b), where a whole spheroid is visible on the fracture surface of a RndA (geometry at highest stress triaxiality), confirms these results. The fact that the spheroid was not cut during the surface polishing proves that the matrix debonding occurred in the out of plane direction also.

Then, the damage model coefficients of the matrix were determined through an optimization procedure using as reference values the global strains at failure under the different stress triaxiality conditions, Table 2. The result of the optimization procedure is shown in the failure locus of Figure 3, where the strain-triaxiality path of the most critical point in the matrix is represented for each specimen geometry. Failure occurs when the strain path crosses the calibrated failure locus.

Finally, the UCM was used to simulate the dynamic tensile tests at a reference strain rate of 1200 s^{-1}, at room temperature. In order to evaluate the influence of the spheroids on the fracture process, strain rate and temperature effects on matrix ductility were not considered. Further, since the global stress-strain is assumed to be an equilibrium state for the UCM, the stress wave transient was not simulated. The main difference compared to the quasistatic configuration lies in the temperature gradients arising from the adiabatic condition. The gradient leads to a redistribution of the stress and strain fields for which the critical condition for the quasistatic configuration (continuous, blue line in Figure 5(a)) is no longer critical for the dynamic configuration. As shown in Figure 4, the critical point moves slightly its position from the interface, point "P1", into the matrix, point "P2", whose corresponding strain path is represented by the dashed, red line in Figure 5(a). To reach the critical condition for failure, additional global strain is needed

TABLE 2. Bonora's damage model coefficients for the ausferrite matrix.

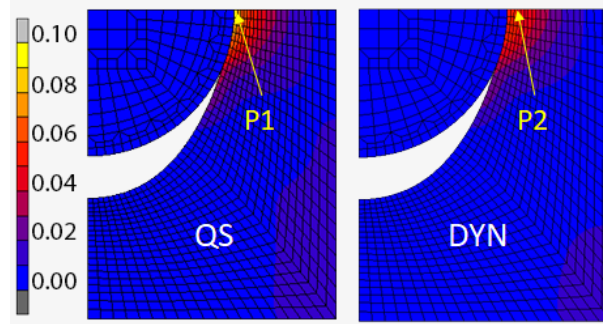| ε_{th}	ε_f	D_{cr}	α
0.10	0.36	0.10	0.30

FIGURE 4. Damage contours and deformation in the unit cell calculated under quasistatic (left) and dynamic (right) condition.
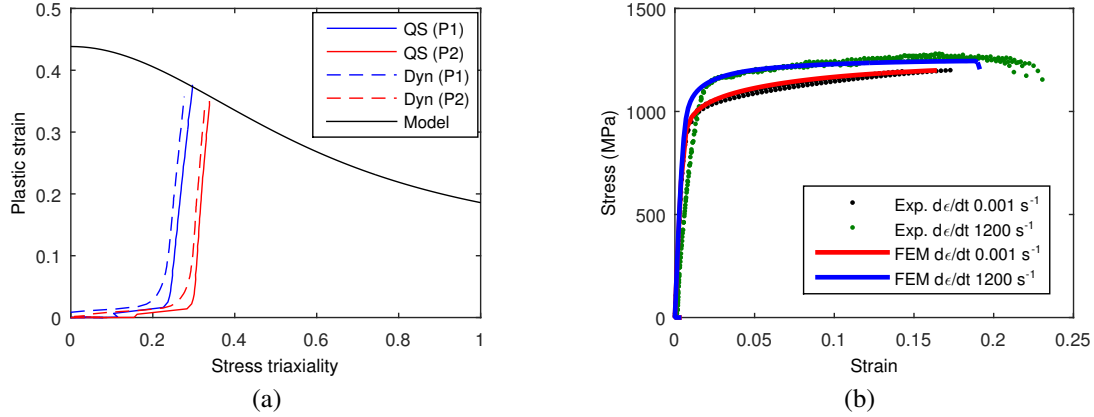

FIGURE 5. (a) Strain-triaxiality paths and matrix failure locus for different strain rates; (b) comparison between experimental and calculated stress-strain curves.

that can be estimated at about 10%. The value is compatible with the increased ductility observed at the macroscale, Figure 5(c).

CONCLUSIONS

Characterization tests performed on ADI JS/1050-6 showed that its ductility increases with temperature and strain rate. If the first effect is expected as a result of a higher matrix ductility, the second, although confirmed by other works, does not have an equally straightforward interpretation. Here, a micromechanics analysis was performed to explore the spheroids role in determining the stress state in the matrix and to investigate how the heterogeneous stress state affects the failure process. An UCM was developed to replicate the periodic microstructure of the ADI. The macroscopic stress triaxiality histories were used as input of the UCM that showed to properly reproduce both the global stress-strain response and the local debonding morphology, under different states of the stress triaxiality. Simulations of dynamic tensile tests demonstrated that the stress field redistribution, due to the adiabatic condition, postpones the failure occurrence, coherently with the increased experimentally observed ductility.

REFERENCES

[1]   R. K. Behera, B. P. Mahto, J. S. Dubey, S. C. Mishra, and S. Sen, International Journal of Minerals, Metal-
        lurgy, and Materials **23**, 40–48 (2016).
[2]   N. Bonora and A. Ruggiero, International Journal of Solids and Structures **42**, 1401–1424 (2005).
[3]   J. Yang and S. K. Putatunda, Materials Science and Engineering: A **382**, 265–279 (2004).
[4]   C. Wadageri and R. Kurahatti, International Journal of Advanced Research in Science and Engineering **5**,
        425–431 (2016).
[5]   F. Zanardi, F. Bonollo, G. Angella, N. Bonora, G. Iannitti, and A. Ruggiero, International Journal of Metal-
        casting **11**, 136–147 (2017).
[6]   S. K. Putatunda, Materials and Manufacturing Processes **25**, 749–757 (2010).
[7]   A. G. Fuller, Materials & Design **6**, 127–130 (1985).
[8]   W. Böhme and L. Reissig, Advanced Engineering Materials **17**, 1189–1196 (2015).
[9]   H. Yamamoto, T. Kobayashi, and H. Fujita, Tetsu-to-Hagane **85**, 765–770 (1999).
[10]   D. Myszka, L. Cybula, and A. Wieczorek, Influence of heat treatment conditions on microstructure and
        mechanical properties of austempered ductile iron after dynamic deformation test, 2014.
[11]   C. Labrecque and M. Gagn, Canadian Metallurgical Quarterly **37**, 343–378 (1998).
[12]   D. F. Adams and D. A. Crane, Computers & Structures **18**, 1153–1165 (1984).
[13]   D. Allen and J. Boyd, ASME AEROSP DIV PUBL AD, ASME, NEW YORK, NY,(USA), 1993 **37**, 31–45
        (1993).
[14]   N. Bonora and A. Ruggiero, Composites Science and Technology **66**, 323–332 (2006).
[15]   G. Iannitti, A. Ruggiero, N. Bonora, S. Masaggia, and F. Veneri, Theoretical and Applied Fracture Mechanics
        (2017).
[16]   N. Bonora, Engineering Fracture Mechanics **58**, 11–28 (1997).
[17]   J. Lemaitre, Journal of Engineering Material and Technology **107**, 83–89 (1985).
[18]   A. Pirondi and N. Bonora, Computational Materials Science **26**, 129–141 (2003).
[19]   N. Bonora, A. Ruggiero, D. Gentile, and S. De Meo, Strain **47**, 241–254 (2011).